ORIGINAL RESEARCH

Design of Montelukast Nanocrystalline Suspension for Parenteral Prolonged Delivery

Jun Soo Park[1], Min Seop Kim[1], Min Yeong Joung[1], Hyun Jin Park[1], Myoung-Jin Ho[1], Jun Hyuk Choi[1], Jae Hee Seo[1], Woo Heon Song[1], Young Wook Choi (ID)[2], Sangkil Lee[3], Yong Seok Choi[1], Myung Joo Kang[1]

[1]College of Pharmacy, Dankook University, Cheonan, Republic of Korea; [2]College of Pharmacy, Chung-Ang University, Seoul, Republic of Korea; [3]College of Pharmacy, Keimyung University, Daegu, Republic of Korea

Correspondence: Myung Joo Kang, College of Pharmacy, Dankook University, Dongnam-gu, Cheonan, 31116, Republic of Korea, Tel +82 41 550 1446, Fax +82 41 550 7899, Email kangmj@dankook.ac.kr

Background: Montelukast (MTK), a representative leukotriene receptor antagonist, is currently being investigated as a potential candidate for treating Alzheimer's disease. For potent and effective dosing in elderly patients, a parenteral prolonged delivery system is favored, with improved medication adherence with reduced dosage frequency.

Purpose: This study aimed to design a nanocrystalline suspension (NS)-based MTK prolonged delivery system and evaluate its pharmacokinetics profile and local tolerability following subcutaneous administration.

Methods: To decelerate the dissolution rate, the amorphous MTK raw material was transformed into a crystalline state using a solvent-mediated transformation method and subsequently formulated into NS using a bead-milling technique. The MTK NSs were characterized by morphology, particle size, crystallinity, and in vitro dissolution profiles. The pharmacokinetic profile and local tolerability at the injection site following subcutaneous injection of MTK suspension were evaluated in rats.

Results: Microscopic and physical characterization revealed that the amorphous MTK powder was lucratively transformed into a crystalline form in acidic media (pH 4). MTK crystalline suspensions with different diameters (200 nm, 500 nm, and 3 μm) were uniformly prepared using bead-milling technology, employing polysorbate 80 as suspending agent. Prepared crystalline suspensions exhibited analogous crystallinity (melting point, 150°C) and size-dependent in vitro dissolution profiles. MTK NSs with particle sizes of 200 nm and 500 nm provided a protracted pharmacokinetic profile for up to 4 weeks in rats, with a higher maximum drug concentration in plasma than the 3 μm-sized injectable suspensions. Histopathological examination revealed that MTK NS caused chronic granulomatous inflammation at the injection site, which resolved after 4 weeks.

Conclusion: The MTK parenteral NS delivery system is expected to be a valuable tool for treating Alzheimer's disease with extended dose intervals.

Keywords: montelukast, parenteral prolonged release delivery, crystallinity, nanocrystalline suspension, bead-milling, pharmacokinetics, local tolerability

Graphical Abstract
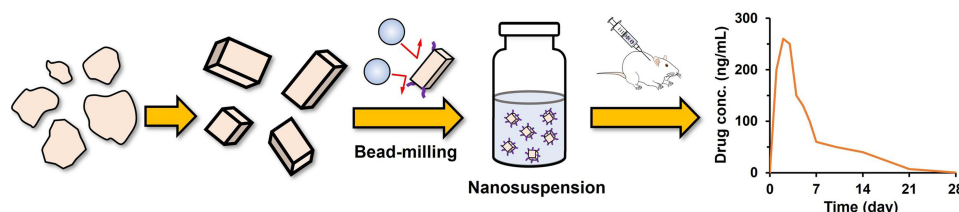
Introduction

Alzheimer's disease (AD) is a prominent neurodegenerative disease characterized by a gradual decline in cognitive ability and memory loss.[1] Although AD's pathogenesis is not completely understood, the tau protein aggregation and intraneuronal neurofibrillary tangle formation, extracellular senile plaques, neuronal loss, microglial, and neuroinflammatory reactions have been considered the main neurodegenerative disease hallmarks.[2–7] Recent studies have supported the positive effect of cysteinyl leukotriene type 1 (cysLT-1) receptor antagonists on inflammatory responses in the brain, neuronal injury, blood-brain-barrier (BBB) integrity, and accumulation of amyloid-β42 (Aβ) protein.[8–10] Montelukast (MTK), a representative leukotriene antagonist, has been prescribed for chronic asthma and seasonal allergy treatment.[10] Oral therapy is being clinically investigated as an alternative medication for Alzheimer's disease.[11–15] MTK is included in oral dosage forms in the amorphous state to provide rapid and profound dissolution and intestinal absorption of the hydrophobic compound (log$P$ value of 8.4).[16] It was rapidly absorbed upon oral administration, exhibiting a maximum plasma concentration (C_{max}) within 3–4 h, with approximately 66% oral bioavailability in healthy subjects.[17] However, when considering its potent prescription for Alzheimer's patients with poor medication adherence, a parenteral prolonged delivery system offering an effective therapeutic level for several weeks following a single administration can be favored with extended dosing intervals.[18] Previously, biodegradable polymeric microparticle system has been designed for prolonged delivery of MTK, providing protracted pharmacokinetic profile over 2 weeks. However, it was quite challenging to administer sufficient MTK dose due to the low drug loading in the particle, with complicated fabrication process.[19]

Drug nanocrystalline suspensions (NSs) have emerged as a promising tool for designing parenteral prolonged delivery system for insoluble drug pharmaceuticals.[20–22] NS is a colloidal dispersion of nanosized drug particles stabilized by a minimal quantity of polymeric and surfactant stabilizers in the continuous phase.[23] The parenteral delivery system provides high drug loading, excellent pharmacokinetic persistence, and ease of scale-up. Following intramuscular or subcutaneous (SC) injection, drug particles gradually dissolve at the injection site and partition into the bloodstream, providing a continuous drug concentration profile over several weeks.[21,24] Moreover, the local inflammatory reaction at the injection site, including macrophage infiltration, phagocytosis of the injected dose, fibrosis, and angiogenesis, affects drug dissolution patterns at the injection site, modulating the pharmacokinetic profile following the drug suspension's SC injection.[25,26]

In the drug suspension-based LA system design, the crystalline state of the drug particles is one of the factors dictating the crystalline suspension's physicochemical stability and pharmacokinetic behavior. The amorphous or thermodynamically unstable forms provide supersaturated solubility profile, showing faster release rates than the stable crystalline form.[27,28] This rapid dissolution of the drug particles promotes the elimination of the drug from the injection site, following SC or intramuscular injection. In addition, the amorphous state of suspended drug particles causes deteriorated chemical stability and recrystallization in the dispersion medium.[29–32] Therefore, stable crystalline solid forms are necessary to formulate parenteral crystalline suspensions with improved physicochemical stability and prolonged pharmacokinetics. Crystalline transformation techniques, such as solid–solid transformations, solution-mediated transformations, transformation via raw material melting, and transformations from drug solutions, are occasionally employed to obtain stable crystalline pharmaceutical solids.[33,34]

Herein, the objectives of the present study were to convert amorphous MTK into its crystalline form using a solution-mediated transformation method and design NS of MTK for prolonged parenteral delivery. MTK NS or microcrystal suspensions (MS) were prepared using lab-scale bead milling and characterized by morphology, particle size, crystallinity, and in vitro dissolution profile. The pharmacokinetic profile following SC injection of drug suspensions with different crystal sizes (200 nm, 500 nm, and 3 μm) was evaluated in rats using validated LC-MS/MS analysis. Moreover, local tolerability and inflammatory responses against MTK NS and MS in rats were histopathologically evaluated.

Materials and Methods
Materials

The sodium salt of MTK was obtained from KyongBo Pharmaceutical Co. Ltd. (Asan, South Korea). MTK and zafirlukast analytical standards were used as internal standards for LC-MS/MS. Polysorbate 80 (P80), tyloxapol,

polyethylene glycol 4000 (PEG 4000), sodium carboxymethylcellulose (Na CMC), polyvinylpyrrolidone (PVP K17), acetic acid, sodium acetate, lactic acid, sodium lactate, and phosphate-buffered saline tablets were purchased from Sigma Chemical Co. (St. Louis, MO, USA). Polyoxyl 15 hydroxy stearate (Kolliphor HS15), polyoxyl-35 castor oil (Kolliphor EL), and polyoxyl 40 hydrogenated castor oil (Kolliphor RH40) were provided by BASF (Ludwigshafen, Germany). HPLC-grade acetonitrile and methanol were purchased from J. T. Baker (Phillipsburg, NJ, USA). All other chemicals were of analytical grade and used without further refinement.

Conversion of Amorphous MTK Powder into Crystalline Form

The amorphous MTK powder was converted into a crystalline form using a solution-mediated transformation procedure.[35] Briefly, approximately 10 g of amorphous weak-acid powder was suspended in 20 mM lactate buffer (pH 4.0) and stored at 60°C for 4 days. The drug suspension was then centrifuged at 3000 rpm to settle the suspended drug particles. The collected drug particles were washed three times with distilled water to remove the lactate buffer and desiccated under light-resistant conditions for 24 h. The prepared drug powder was stored in a glass vial at room temperature to prepare injectable suspensions.

Preparation of MTK NS and MS Using a Bead-Milling Process

MTK-loaded crystalline suspensions were fabricated by pulverizing the drug powder into fine particles in an aqueous vehicle using a lab-scale bead-milling technique.[36,37] Approximately 5–20 mg (0.5–2.0%, w/v) of the suspending agent (Table 1) and 9 mg (0.9%, w/v) of sodium chloride as an isotonic agent were dissolved in an aqueous vehicle (20 mM acetate buffer, pH 5.0). Subsequently, 100 mg of MTK and 1 g of zirconia beads (0.3 mm) were added to the aqueous vehicle and pre-wetted for 5 min using a vortex shaker at room temperature. The coarse dispersion was bead-milled using the ZentriMix 380R (Andreas Hettich GmbH und Co KG, Tuttlingen, Germany) at different speeds (500, 1000, and 1500 rpm) for 2 h. For every milling trial, the cooling device was set to −10°C to prevent temperature elevation and MTK thermal degradation during the fabrication procedure. The prepared crystal suspensions were separated from the beads and placed in light-protective scintillation vials.

Table 1 Effect of Steric Stabilizer on Particle Size, Homogeneity, and Dispersibility of MTK Crystalline Suspensions

Stabilizer[a]	Appearance	Particle Size (μm)[b]	Homogeneity[b]
P80	Homogeneous	0.26 ± 0.01[c]	0.35 ± 0.00[e]
Poloxamer 188	Homogeneous	3.68 ± 0.21[d]	1.64 ± 0.20[f]
Solutol HS15	Homogeneous	8.65 ± 0.23[d]	7.05 ± 2.72[f]
Cremophor EL	Homogeneous	3.56 ± 0.16[d]	1.40 ± 0.08[f]
Cremophor RH40	Homogeneous	3.97 ± 0.08[d]	1.61 ± 0.02[f]
Tyloxapol	Homogeneous	5.37 ± 0.02[d]	2.36 ± 0.02[f]
PEG 4000	Homogeneous	10.69 ± 0.14[d]	3.38 ± 0.26[f]
Sodium CMC	Homogeneous	14.70 ± 0.37[d]	2.31 ± 0.14[f]
PVP K17	Homogeneous	3.64 ± 0.01[d]	1.84 ± 0.01[f]

Notes: [a]The stabilizer concentration in the aqueous vehicle was set to 1.2% w/v with a milling speed of 1500 rpm. [b]Data represent mean ± SD. [c]Indicates the mean hydrodynamic size determined using dynamic light scattering measurement technology (Zetasizer Nano® Instruments). [d]Shows the median particle size (d_{50}) determined using a laser diffraction particle size analyzer (Mastersizer MS2000). [e]Polydispersity index, calculated by dividing the square of the standard deviation by the mean particle diameter. [f]Span, calculated by dividing the difference between d_{90} and d_{10} by d_{50}. d_{90}, d_{10}, and d_{50} indicate the proportions of particles with diameters smaller than 90, 10, and 50%, respectively.
Abbreviations: MTK, montelukast; P80, polysorbate 80; PEG 4000, polyethylene glycol 4000; CMC, carboxymethylcellulose; PVP K17, polyvinylpyrrolidone K17.

Characterizations of MTK Powder and Crystalline Suspensions

Morphological Observation

The morphological features of MTK raw materials and drug crystals dispersed in the aqueous vehicle were examined using scanning electron microscopy (SEM, Model JSM-6510, JEOL, Tokyo, Japan). Ten times-diluted MTK NS samples were loaded onto an aluminum stub using double-sided carbon tape (Sungho sigma, Suwon, Korea) and dried at room temperature for 2 h to remove the aqueous vehicle. MTK raw materials and desiccated drug crystals on the stub were then coated with a thin platinum layer using an automatic sputter coater (Model 108AUTO, Cressington, UK) at 15 mA for 10 min. Microphotographs of the coated samples were obtained at an acceleration voltage of 20 kV.

Polarized Microscopic Observation

A polarized light microscopy system (BX51, Olympus, Tokyo, Japan) was used to evaluate the crystallinity of MTK raw material after crystallinity transformation process. The drug powder was spread on a glass slide and covered with a glass slip. The specimens were visualized for the presence of birefringence under polarized light and photographed using a digital GXCAM-3 camera (GX Optical). All images were captured at room temperature with an exposure time of 0.2 s.

X-Ray Diffractometry (XRD)

The raw materials' and NS formulas' XRD patterns were recorded on an X-ray diffractometer (Ultima IV, Rigaku Corporation, USA) using CuKα radiation with λ = 1.54 Å (40 kV and 35 mA).[38] Drug powder and desiccated drug crystals were placed on a flat aluminum sample holder and scanned from 5° to 60° with a step size of 0.02° and scanning speed of 2 s/step.

Thermal Analysis

Thermal behavior of raw material and formulations was evaluated using DSC (DSC 50, Shimadzu Scientific Instruments (MD)). The crystalline suspensions were dried in an oven at 60°C for 12 h. Each sample in solid-state (approximately 2 mg) was placed in a standard aluminum pan and sealed with a lid. The phase transition of each sample was recorded at a heating rate of 10°C/min with a nitrogen purge of 20 mL/min. An empty aluminum pan was used as a reference.

Drug Content Analysis

The MTK raw material content before and after the crystalline conversion procedure and the crystalline suspension drug content were determined using HPLC analysis.[39] Solid-state MTK raw material (10 mg) and crystalline suspension (100 μL) were dissolved in acetonitrile, diluted 2-fold with the mobile phase, and analyzed using HPLC. On the other hand, to determine the amount of MTK dissolved in the suspension, each sample (1 mL) was centrifuged at 13,000 rpm for 10 min, and the supernatant was diluted 2-fold with the mobile phase and analyzed using HPLC. The MTK quantity suspended in aqueous vehicles was estimated by subtracting the MTK amount dissolved from the total amount in the suspension.

The MTK concentration in the samples was analyzed using Shimadzu HPLC composed of a pump (Model 515 pump), a UV–VIS (ultraviolet-visible) detector (Model 486), and an autosampler (Model 717 plus) equipped with a C18 column (4.6 mm I.D. × 250 mm, 5 μm, Waters, USA). The mobile phase consisted of 3:2 (v/v) distilled water and acetonitrile (pH 2.5, 1.5% v/v trifluoroacetic acid) at a rate of 1.0 mL/min. The injection volume and column temperature were set at 20 μL and 30°C, respectively. The eluent was monitored at a wavelength of 230 nm. The MTK retention time was approximately 4.5 min. The calibration curve for MTK plotted between analyte concentration and the area under the peak was linear (y = 46497x + 4473.4, r^2=1) (1–100 μg/mL). The limit of quantification (LOQ) values was 1 μg/mL.

Determination of Size Distribution of MTK Crystalline Suspensions

The mean particle size and polydispersity index (PDI) of the MTK-loaded NSs were determined using Zetasizer Nano® Instruments (Malvern Instruments, UK).[40,41] Each sample (100 μL) was diluted 10-fold with DW and then loaded onto disposable cells. The NS size distribution was analyzed using a 4 mW He-Ne laser (633 nm) at 25°C, with a 90° scattering angle. In contrast, the MTK MS particle size and uniformity, determined to be over 1000 nm in the preliminary Zetasizer Nano® analysis, were evaluated using a laser diffraction particle size analyzer (Model Mastersizer MS2000, Malvern Instruments Ltd., UK). After background alignment with each dispersion medium, each sample was added dropwise to the

Hydro 2000S automatic dispersion unit until the obscuration value reached 20–30%. Samples and backgrounds were analyzed five times, and size distributions by volume were calculated by applying the Mie theory. The refractive index of the aqueous vehicle was set as 1.33. The median value (d_{50}) was defined as the diameter at which half of the population was below this value. Similarly, 90% of the distribution was below the d_{90} value, and 10% of the population was below the d_{10} value. The homogeneity of the MTK particles suspended in the vehicle was estimated by determining the SPAN value, which was calculated by dividing the difference between d_{90} and d_{10} by d_{50}.[42]

Osmolality and pH Determination
The osmolality (mOsm/kg) and pH of MTK-loaded injectable suspension were directly determined using an osmometer (Micro-osmometer 210, Fiske Associates, Norwood, MA, USA) and pH meter (S220, Mettler-Toledo LLC, Columbus, OH, USA), respectively, without dilution.

In vitro Dissolution Profile of Drug Powder and Crystalline Suspensions
The in vitro MTK dissolution profile from crystalline suspensions was comparatively evaluated using a shaking dissolution tester (Model BF-60SIR; Biofree, Seoul, Korea). MTK raw materials pulverized below 10 μm (10 mg) were added to 200 mL of phosphate-buffered saline (pH 7.4, 10 mM of phosphate buffer and 137 mM of NaCl) maintained at 37°C and stirred at 110 rpm. Concerning MTK crystalline suspensions, MTK suspensions (500 μL) with d_{50} values of 200 nm, 500 nm, and 3 μm were spiked into the 200 mL of dissolution media maintained at 37°C and stirred at 110 rpm. 1.0% w/v P80-admixed phosphate-buffered saline (pH 7.4) was used as the dissolution medium to guarantee sink conditions. At predetermined times, 1 mL of dissolution medium was collected and centrifuged at 13,000 rpm for 10 min to remove withdrawn MTK particles. The drug particles were then added to dissolution media with the fresh dissolution medium kept at 37°C. The supernatant was diluted 4-fold with methanol and analyzed using HPLC as described previously.

In vivo Pharmacokinetic Profile of MTK Crystalline Suspensions in Rats
The in vivo MTK pharmacokinetic profile following SC crystalline suspension administration was determined in normal rats. The animal study was performed in accordance with guidelines for the care and use of laboratory animals of Dankook University after approval from the Institutional Animal Care and Use Committee (IACUC) of Dankook University (Cheonan, Korea) (DKU-19-032, 8th October 2019). Sprague-Dawley rats (male, 150–200 g, 6-week-old) obtained from Samtako Bio Korea (Gyeonggi-do, Korea) were housed under temperature (23 ± 1°C) and light cycle (day/night: 12 h) with free access to food and water. The acclimatized rats were randomly divided into three groups (200 nm NS, 500 nm NS, and 3 μm MS) (n = 5 per group). Each group was administered an injectable suspension subcutaneously using a 31 G insulin syringe (30 mg/kg as MTK). Blood samples (approximately 600 μL) were collected from the jugular vein 3, 6, 10, 24, 48, 96, 168, 240, 336, 604, and 772 h after injection. The blood samples were centrifuged at 4000 rpm for 10 min. The plasma samples were then stored at −70°C before HPLC-MS/MS analysis. After thawing at ambient temperature, the plasma MTK level was determined by HPLC-MS/MS, as previously described.[43]

Pharmacokinetic parameters, such as the area under the plasma concentration versus the time curve from 0 to 28 days ($AUC_{0-28days}$), maximum plasma concentration (C_{max}), time to peak maximum plasma concentration (T_{max}), and half-life ($T_{1/2}$), were calculated using a pharmacokinetic analysis program (WinNonlin® version 5.2, Pharsight Co., Mountain View, CA).

In vivo Histological Observation of Injection Site Following SC Injection in Rats
The in vivo local inflammatory responses in subcutaneous tissue following a single MTK suspension injection were evaluated in 6-week-old male normal Sprague-Dawley rats (200 ± 20 g) after approval by the Institutional Animal Care and Use Committee (IACUC) of Dankook University (approval number: DKU-19-033, date of approval: October 8, 2019). After an acclimatization period of at least 3 days, three different MTK suspensions (200 nm NS, 500 NS, and 3 μm MS) were injected into subcutaneous regions of the loose skin over the neck at a dose of 30 mg/kg, equivalent to the MTK dose for pharmacokinetic evaluation. At predetermined time points (4, 7, 14, and 28 days after administration), rats

were sacrificed by CO_2 asphyxiation. Subcutaneous tissues over an area of 4 cm^2 were excised surgically. Dissected subcutaneous tissues were secured at each edge with a pin and then fixed in 10% neutral-buffered formalin for 72 h. The fixed tissues were dehydrated using an ascending ethanol gradient (70, 80, 95, and 100%), cleared with xylene, and embedded in paraffin wax under conventional conditions (40°C, 400 mm Hg, shaking at 100 rpm). The specimens embedded in paraffin wax were then sectioned at a thickness of 20 μm using a microtome (Model Leica RM2165, Wetzlar, Germany). The sliced sections were washed twice with xylene to remove paraffin and dehydrated through a decreasing ethanol gradient (100, 95, 80, and 70%). The sections were stained with hematoxylin and eosin (H&E) and mounted onto slides covered with a mounting medium (Canadian balsam mounting solution).

The H&E-stained samples were then scrutinized and digitalized using a Pannoramic 250 Flash digital microscope (P250 Flash digital microscope; 3DHISTECH, Budapest, Hungary) equipped with CaseViewer software (3DHISTECH, Budapest, Hungary). The injected subcutaneous tissues' histopathological evaluation included the shape of the depot and inflammatory cells such as lymphocytes, macrophages, angiogenesis, necrosis, and fibrosis.

Quantification of Inflammatory Cells Infiltrated at the Injection Site

For a more quantitative analysis of the local inflammatory response following SC MTK suspension injection, the degree of cellular infiltration (polymorphonuclear cells, lymphocytes, macrophages, etc.) into injection sites was further analyzed using QuPath software (ver. 0.2.3; Queen's University, Belfast, Northern Ireland, UK).[44–46] First, the injection site's inflammatory area was determined using the wand tool in QuPath by bordering the depot area contour; the bordered area was automatically calculated using the program. The number of inflammatory cells in the depot was counted using the QuPath cell detection tools. The threshold, maximum background intensity, and nucleus parameters were set to 0.2 μm, 2.0, and 5–400 μm^2, respectively.

Statistical Analysis

All the experiments were repeated at least three times, and the data were expressed as mean ± standard deviation (SD). The differences were evaluated by one-way analysis of variance (ANOVA) and Tukey's post-hoc tests (SPSS, version 22.0, Chicago, IL, USA). Statistical significance was set at $p < 0.05$.

Results and Discussion

Conversion of Amorphous Raw Material into Crystalline Form

To impede the dissolution rate of the cysLT-1 receptor antagonist and attain a prolonged dissolution profile from an injectable drug suspension, the amorphous MTK powder was attempted to transform into a stable crystalline form. Solid-state conversions of pharmaceutical compounds can be classified according to their underlying mechanisms as solid–solid transformations, solution-mediated transformations, transformations via active ingredient melting, and transformations from active ingredient solutions.[47] Herein, amorphous MTK powder transformation into a stable crystalline form was promoted using solid-state transformation in the presence of a solvent, a solvent-mediated transformation method. The weak-acid amorphous MTK powder suspended in an acidic medium (pH 4) and was heated at 60°C to induce conversion into crystalline form. As the amorphous state is thermodynamically unstable, its crystal nucleation and growth might be facilitated by elevated temperature, humidity, and solvent effects.[48]

MTK's crystalline transformation in acidic media was estimated using SEM, polarized light microscopy (PLM), DSC, and XRD. SEM observations revealed that amorphous MTK particles with no distinctive shape (Figure 1A) were converted into distinctive and angular-shaped particles by crystallization (Figure 1B). Under polarized microscopic observation, the amorphous raw material with no marked birefringence (Figure 1C) was rehabilitated into birefringent microparticles (Figure 1D). This indicated that the amorphous MTK particle conversion into semicrystalline and/or crystalline form and crystal growth was drastically augmented under stress conditions.

The transformation into the crystalline form of the MTK powder was further checked by evaluating the thermal behavior and XRD patterns. In the DSC experiment, no distinct endothermic peak was observed in the amorphous raw material; in contrast, a sharp peak around 150°C was observed in MTK powder obtained during the crystallization
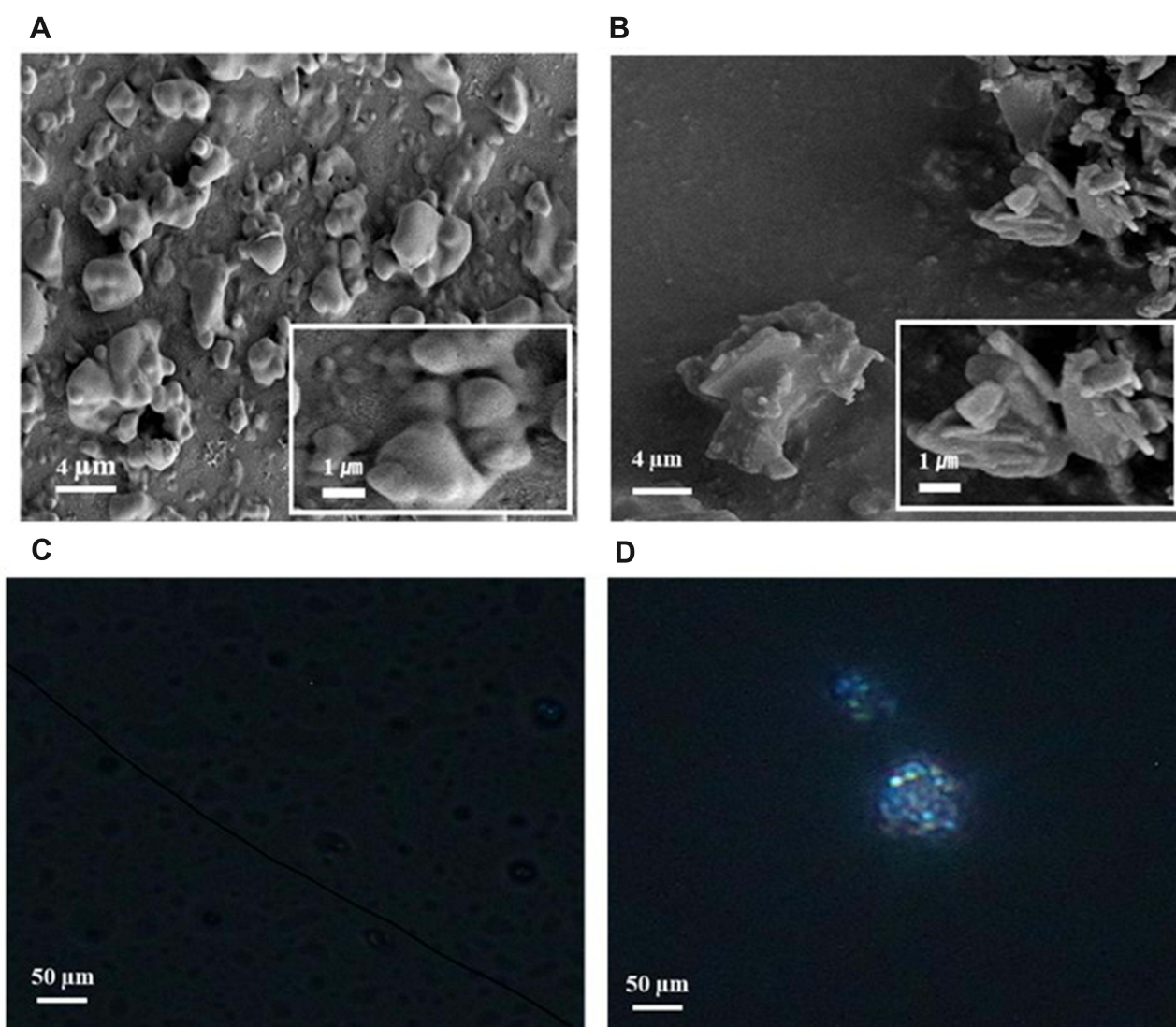
Figure 1 Morphological observation of MTK raw materials. SEM images of MTK raw materials (**A**) before and (**B**) after crystallization. Polarized images of the raw materials (**C**) before and (**D**) after crystallization.
Abbreviations: MTK, montelukast; SEM, scanning electron microscope.

process (Figure 2A). The amorphous drug conversion into its crystalline form was further evaluated using XRD. When X-rays irradiate solid-state materials, they are scattered by the electrons revolving around the nucleus of atoms. The unique interference between scattered waves provides an orderly arrangement (periodicity) of the crystalline materials' atomic structure. No noticeable diffraction pattern was observed at 5–40° in the amorphous MTK powder. In contrast, sharp peaks were observed at 10°, 15°, 20°, and 25° in the MTK powder processed by the solid-state conversion process (Figure 2B). During incubation, there was no change in drug content in an acidic medium for crystalline conversion in HPLC analysis (Figure 2C). From these findings, we concluded that the amorphous MTK powder was effectively converted into a crystalline form with no drug degradation under the solution-mediated transformation procedure.

Next, the alternation in the dissolution rate after conversion to the crystalline form was evaluated under physiological conditions (phosphate buffer, pH 7.4) (Figure 2D). The amorphous MTK powder showed a supersaturated dissolution pattern, with apparent solubilities of 18, 29, 51, and 2.2 μg/mL after 2, 4, 8, and 24 h, respectively. Conversely, a crystalline form conversion resulted in a sharp decrease in the dissolution rate under physiological conditions; the apparent MTK solubility was determined to be 2.5, 2.7, 6.3, and 1.9 μg/mL after 2, 4, 8, and 24 h, respectively. The
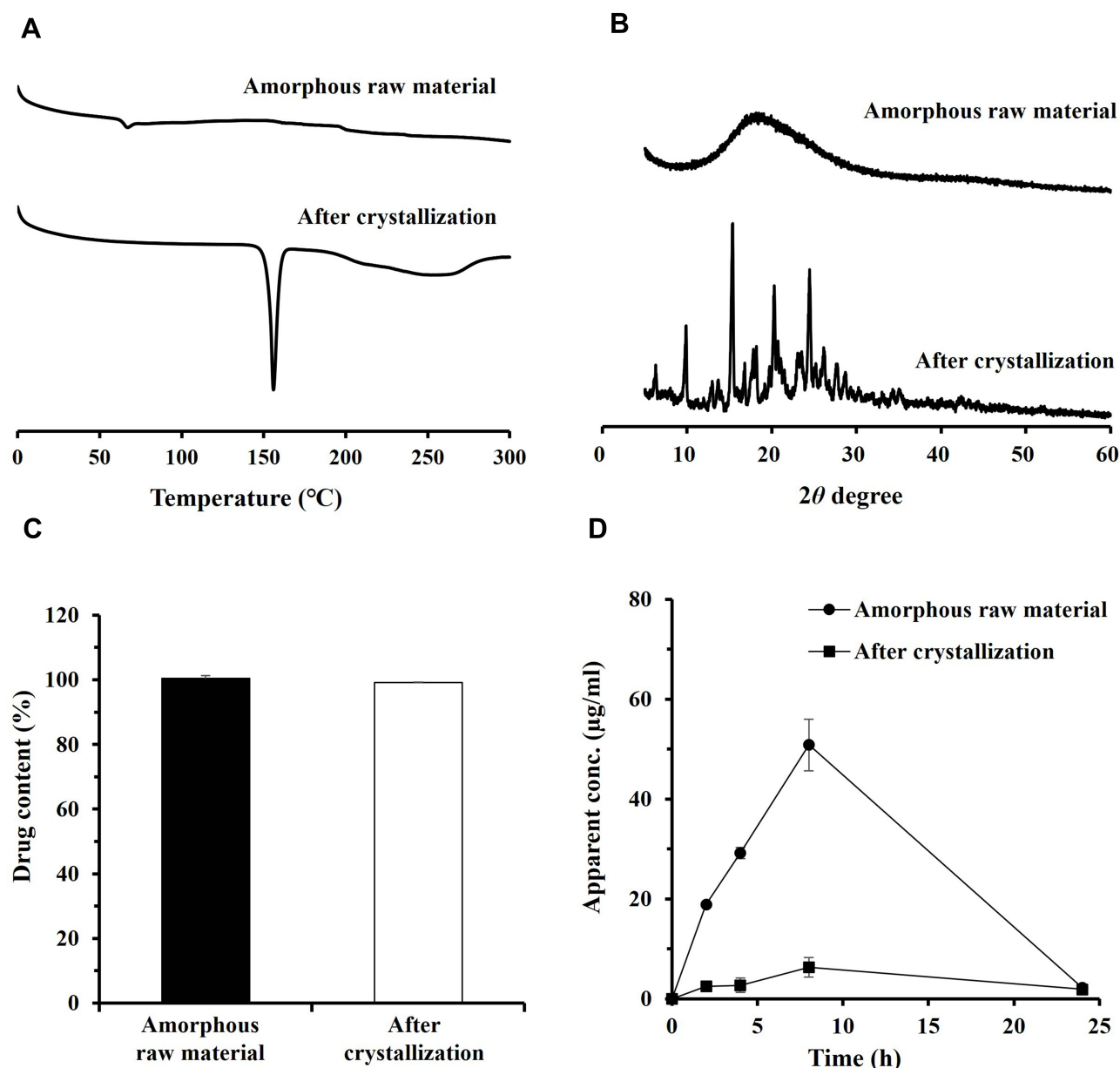
Figure 2 Alternation in MTK raw material physicochemical characteristics after crystallization. (**A**) DSC curves, (**B**) XRD patterns, and (**C**) drug content of MTK raw materials after crystallization. (**D**) Apparent concentration profile of MTK raw materials in aqueous media (phosphate buffered saline, pH 7.4) after crystallization.
Note: Data in (**C**) and (**D**) represent mean ± SD (n = 3).
Abbreviations: MTK, montelukast; DSC, differential scanning calorimetry; XRD, X-ray diffractometer.

drastically delayed dissolution rate by conversion to the crystalline form was expected to prevent supersaturation of MTK particle during bead-milling-based fabrication and enable decelerated dissolution at the injection site.

Screening of Suspending Agent of MTK Crystalline Suspension

MTK-loaded NS and MS were fabricated using a wet milling technique, a top-down approach, decreasing the coarse MTK raw material to sub-micron dimensions in an aqueous vehicle. Mechanical grinding using media milling beads has the following advantages: low energy utilization, ease of scale-up, no organic solvent use, and minimum batch-to-batch variation compared to other nanosizing techniques.[49–52] Dual centrifugation, a wet ball milling lab-scale type, pulverizes the raw material by additional sample rotation during the centrifugal process with zirconia beads, resulting in vigorous movement of the samples inside the vials with beads. This eventually results in their rapid homogenization or milling.

DC is a promising tool for the rapid and broad screening of suitable polymers and surfactants for nano-milling poorly soluble drug compounds. Hagedorn et al demonstrated that dual centrifugation is ideal for nano-milling poorly water-soluble compounds in closed disposable containers with small sample sizes.[37] Furthermore, Hagedorn et al reported that the milling results obtained through the dual centrifugation method were comparable to those obtained using larger-scale agitator mills.[37] The MTK crystalline suspension was designed to be administered by SC injection, as medications injected subcutaneously are absorbed more deliberately with reduced flocculation in plasma level compared to intramuscular route, with fewer blood vessels beneath the skin.[53,54] Moreover, it also enables self-administration in patients. In designing the crystal suspension, the drug concentration in the system was set to 100 mg/mL. When the crystal suspension was prepared at a concentration higher than 150 mg/mL, the viscosity of the suspension markedly increased, causing difficulties in SC injection via a 26 G syringe. Nevertheless, considering that up to 1.5 mL of dosing volume is available for SC injection, the novel injectable system can provide a bolus dose equivalent to 2 weeks of oral MTK therapy in clinical trials.[14]

Table 1 presents the particle size and homogeneity of MTK suspension fabricated using different stabilizers. While screening the suspending agent, their concentrations in the vehicle and stirring rate were fixed at 1.2 mg/mL and 1500 rpm, respectively. When poloxamer 188, Solutol HS15, Kolliphor EL, Kolliphor RH40, tyloxapol, PEG 4000, sodium CMC, and PVP K17 were employed, crystal size in suspension was over 3.6 μm, suggesting that the MTK powder was not effectively diminished during the fabrication procedure. In contrast, when P80 was introduced as a suspending agent, MTK particles with a hydrodynamic size of 260 nm were uniformly fashioned with low PDI value. The result suggests that oleic acid, the hydrophobic portion of P80, covers the drug particle surface; simultaneously, the hydrophilic polyethylene moiety moves toward the aqueous solution, effectively reducing interfacial tension. Therefore, P80 was chosen as the suspending agent, and the MTK crystal size was further controlled by adjusting the dispersant concentration and bead-milling intensity.
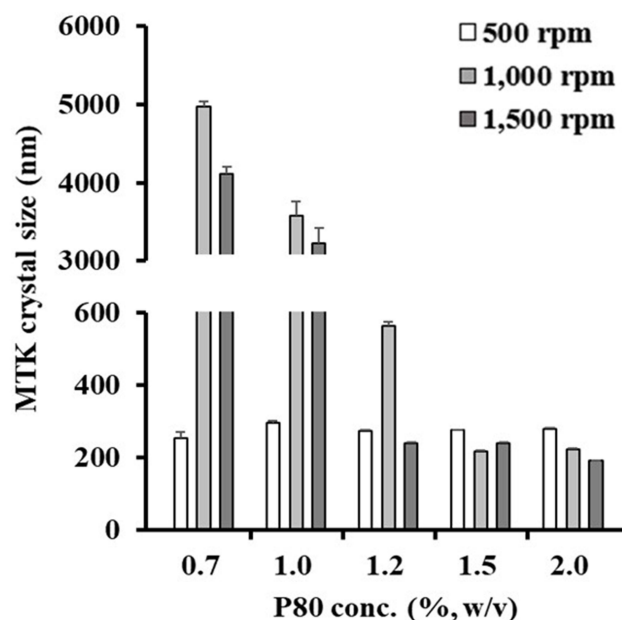
Control of Particle Size of MTK Crystalline Suspension

The particle size and uniformity of MTK crystalline suspension were fine-tuned by adjusting P80′s concentration or the bead-milling conditions (Figure 3). Uniform NSs with sizes ranging from 190 to 230 nm were fabricated using milling intensities of 500 rpm, with no marked difference in the P80 concentration (0.7–2.0 mg/mL). On the other hand, when the milling intensity was fixed at 1000 or 1500 rpm, the particle size was dependent on the P80 concentration, and the crystal size was determined to be 4970, 3570, 560, 220, and 220 nm with P80 concentrations of 0.7, 1.0, 1.2, 1.5, and 2.0%, respectively, and a milling intensity of 1000 rpm. In vigorous milling conditions with milling speed over 1000 rpm, MTK powder would be effectively pulverized into nanoparticles. However, in an environment where sufficient suspending agent to lower the interfacial tension between particles and medium was not provided, thermodynamically unstable drug nanoparticles would be aggregated or form larger particles by Ostwald ripening phenomenon. It has been reported that the mitigation of aggregation and/or Ostwald ripening can be affected by the type and concentration of the suspending agent.[55,56] On the other hand, when the dispersant concentration was sufficient over 1.5%, the fine nanocrystals were preserved with no aggregation. Based on these findings, MTK crystalline suspensions with particle sizes of 200, 500, and 3000 nm were fabricated using the bead-milling technique for further experiments.

Morphological and Physical Characteristics of MTK Crystalline Suspensions

We designed three different MTK formulations with varying particle diameters (200 nm, 500 nm, and 3 μm) (named 200NS, 500NS, and 3MS, respectively), and their morphological and physicochemical properties were characterized by morphology, drug content, particle size, and crystallinity (Table 2 and Figure 4). All MTK suspensions were prepared at a concentration of approximately 100 mg/mL (96.7–105.0 mg/mL), and more than 99.8% of MTK remained as solid-state drug particles in an aqueous vehicle. The particle size of MTK suspensions was determined to 254 nm (named 200NS), 561 nm (500NS), and 3.2 μm (3MS), respectively, with appropriate homogeneity. The MTK crystalline suspension was within the size range of commercialized long-acting crystalline suspensions. The mean particle size of aripiprazole (Abilify maintena®, Otsuka Pharmaceutical Inc., Tokyo, Japan), paliperidone palmitate (Invega sustenna®,

Figure 3 Effect of process variables, including the concentration of suspending agent (P80, 0.7–2.0 w/v%) and milling speed (500–1500 rpm) on MTK crystalline suspension particle size.
Note: Data represented mean ± SD (n = 3).
Abbreviations: P80, polysorbate 80; MTK, montelukast.

Janssen, NJ, US), olanzapine (Zyprexa Relprevv®, Eli Lilly, Indianapolis, IN, USA), and rilpivirine suspensions (Cabenuva®, ViiV Healthcare, GL, UK) was reported to be 1–10 μm,[57] <1000 nm,[58] <3 μm,[59] and <500 nm,[60] respectively. The MTK suspension was isotonic (306–323 mOsm/kg), enabling minimal irritation or pain in the subcutaneous tissue following injection. Nanocrystalline suspensions including 200NS and 500NS have a lower viscosity compared to microcrystals (3MS), making them easy to administer through 31 G syringe needle (data not shown).

SEM observations revealed that the nanocrystals (200NS, 500NS) retained the crystalline raw material's angular shape. The observed crystal size was analogous to that measured using Mastersizer (Figure 4A and B). In the XRD evaluation, both nanocrystals and microcrystals maintained the unique pattern of the crystalline raw materials, despite partial reduction in the intensity (Figure 4C). Thermal analysis also showed that a slight shift in the endothermic peak, which might be attributed to a partial amorphization of the drug by nanomilling process or partial dissolution of MTK by residual P80 onto the drug crystals.[61] Nevertheless, nanocrystals and microcrystals exhibited an obvious melting point of

Table 2 Physicochemical Characteristics of MTK NSs and MS

	200NS	**500NS**	**3MS**
Drug conc. (mg/mL)	103.1 ± 2.7	96.7 ± 5.9	105.0 ± 1.2
Suspended (mg/mL)	102.9 ± 2.7	96.5 ± 5.9	105.0 ± 1.2
Dissolved (mg/mL)	0.02 ± 0.00	0.02 ± 0.01	0.01 ± 0.00
Particle size (nm)	254.3 ± 15.5[a]	561.3 ± 13.1[a]	3229.6 ± 191.5[b]
Homogeneity	0.40 ± 0.01[c]	0.32 ± 0.00[c]	1.83 ± 0.01[d]
Osmolarity (mOsmol/kg)	306.3 ± 4.2	313.3 ± 1.2	323.0 ± 1.6
pH	5.21 ± 0.00	5.2 ± 0.02	5.19 ± 0.01

Notes: [a]Indicates the mean hydrodynamic size determined using dynamic light scattering measurement technology (Zetasizer Nano® Instruments). [b]Indicates the median particle size (d_{50}) determined using a laser diffraction particle size analyzer (Mastersizer MS2000). [c]Polydispersity index, calculated by dividing the square of the standard deviation by the mean particle diameter. [d]Span, calculated by dividing the difference between d_{90} and d_{10} by d_{50}. d_{90}, d_{10}, and d_{50} indicate the proportions of particles with diameters smaller than 90, 10, and 50%, respectively. Data are expressed as mean ± SD (n = 3).
Abbreviations: MTK, montelukast; NS, nanocrystalline suspension; MS, microcrystalline suspension; drug concentration, drug concentration.
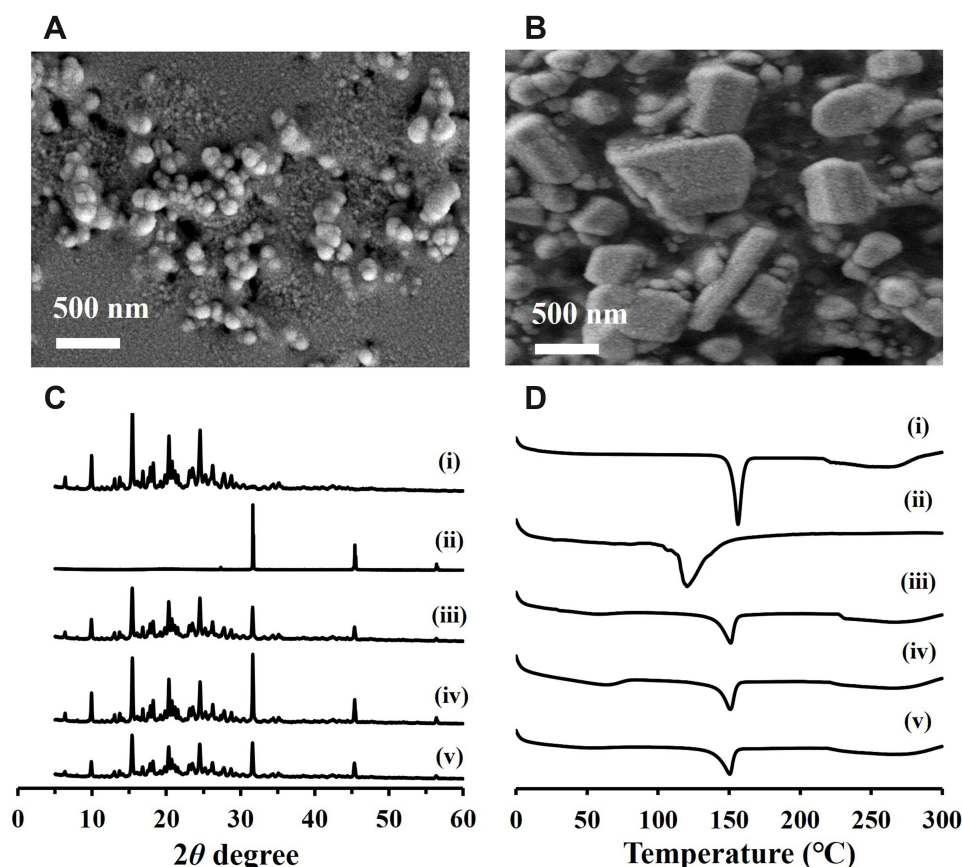
Figure 4 Morphological and physical characteristics of MTK crystalline suspensions with different particle sizes. SEM images of (**A**) 200NS and (**B**) 500NS. Representative (**C**) XRD patterns of (i) crystallized MTK raw material, (ii) vehicle (acetate buffer solution with P80), (iii) 200NS (c), (iv) 500NS, and (v) 3MS, and (**D**) DSC curves of (i) crystallized MTK raw material, (ii) vehicle (acetate buffer solution with P80), (iii) 200NS, (iv) 500NS, and (v) 3MS.
Abbreviations: MTK, montelukast; SEM, scanning electron microscope; XRD, X-ray diffractometer; DSC, differential scanning calorimeter; P80, polysorbate 80; 200NS, 200 nm-sized nanocrystalline suspensions; 500NS, 200 nm-sized nanocrystalline suspensions; 3MS, 3 μm-sized microcrystalline suspension.

150°C, comparable to that of crystalline raw materials (Figure 4D). Based on these findings, we concluded that the MTK crystalline raw material was effectively formulated into nanocrystals and microcrystals, with no alternation in crystalline form through the bead-milling process.

In vitro Dissolution Profile of MTK Crystalline Suspensions

In vitro dissolution pattern of MTK suspensions (200NS, 500NS, and 3MS) was comparatively evaluated under sink conditions (Figure 5). P80 was added to phosphate-buffered saline to provide sufficient MTK water solubility by incorporating the hydrophobic compound into the micelle structure above the critical micelle concentration.[62] The equilibrated MTK solubility in 1 w/v% P80 phosphate-buffered saline was determined to 218 μg/mL (data not shown), which is adequate solubility to provide sink condition.

NS and MS showed biphasic dissolution patterns, characterized by an initial rapid dissolution of over 50%, followed by gradual dissolution. In particular, 200NS and 500NS possessing a larger contact area resulted in more rapid dissolution, exhibiting over 85% drug release after 5 h. There was no significant difference in the dissolution rate under sink conditions between the 200 and 500 NS. In contrast, 3MS exhibited a retarded release profile, with >85% drug release over 48 h. This dissolution pattern can be explained by the Noyes-Whitney equation: dM/dt=k•S•Cs, where dM/dt is the dissolution rate, k is the rate constant, and S is the surface area of the drug particle, Cs, and the drug solution reduction.[63,64] The drug particle size reduction led to a marked increase in surface area, thereby promoting MTL dissolution in the dissolution media. Moreover, the reduction in particle size further promoted drug dissolution, by
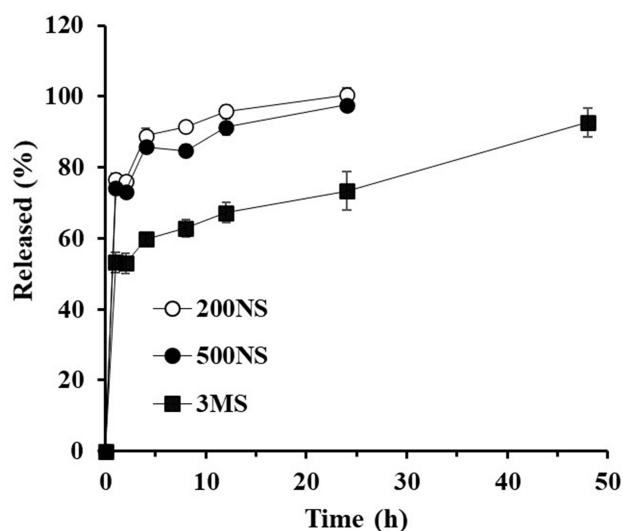
Figure 5 In vitro dissolution profile of MTK from 200NS, 500NS, and 3MS under sink conditions. Sink condition was ensured by adding P80 (1.0%w/v) to phosphate-buffered saline (pH 7.4).
Abbreviations: MTK, montelukast; 200NS, 200 nm-sized nanocrystalline suspensions; 500NS, 200 nm-sized nanocrystalline suspensions; 3MS, 3 µm-sized microcrystalline suspensions.

increased saturation solubility as described by Freundlich–Ostwald equation.[65] Afterwards, the dissolution rate of both NS and MS markedly decelerated, probably due to the decrease in the concentration gradient and residual drug amount. This initial rapid release followed by gradual release profile in NS system has been reported in previous reports.[66–68]

In vivo Pharmacokinetic Evaluation in Rats

The plasma concentration–time profile of MTK following SC injection of different MTK suspensions (200NS, 500NS, and 3MS) is shown in Figure 6. The parameters calculated from the pharmacokinetic profiles are presented in Table 3.
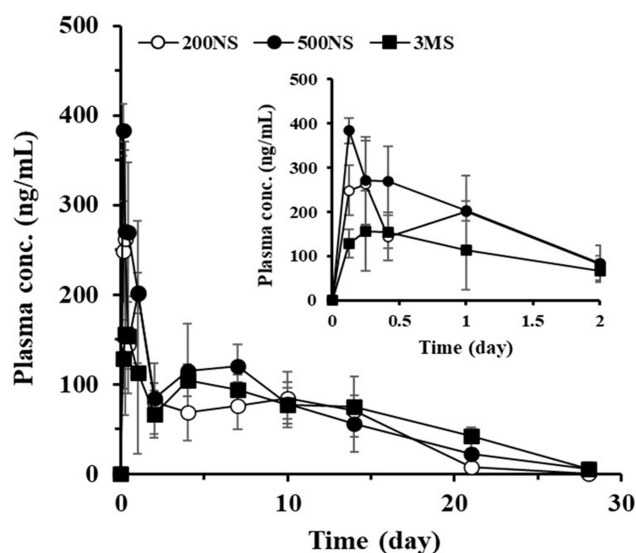
Figure 6 Plasma concentration-time profiles of MTK following SC injection of MTK crystalline suspensions with different particle sizes; 200NS, 500NS, and 3MS in rats.
Note: Data represent mean ± SD (n = 5).
Abbreviations: MTK, montelukast; SC, subcutaneous; 200NS, 200 nm-sized nanocrystalline suspension; 500NS, 200 nm-sized nanocrystalline suspension; 3MS, 3 µm-sized microcrystalline suspension; plasma concentration, plasma concentration.

Table 3 Pharmacokinetic Parameters of MTK Following SC Administration of MTK Crystalline Suspensions with Different Particle Sizes in Rats at a Dose of 30 Mg/Kg

Parameters	200NS	500NS	3MS
C_{max} (ng/mL)	298.0 ± 64.4	383.7 ± 28.8	207.1 ± 78.1
T_{max} (day)	0.4 ± 0.3	0.1 ± 0.0	1.2 ± 1.4
$AUC_{(0-28\ days)}$ (ng ·day /mL)	1418.3 ± 379.3	1737.2 ± 320.0	1533.5 ± 392.5
$AUC_{(0-28\ days)}$ (ng·day/mL)	1420.3 ± 379.6	1832.2 ± 412.2	1563.7 ± 435.8
$T_{1/2(\alpha)}$ (day)[a]	0.2 ± 0.1*	0.8 ± 0.1*	3.7 ± 1.1
$T_{1/2(\beta)}$ (day)[b]	4.0 ± 0.5	5.2 ± 2.3	7.8 ± 3.6

Notes: [a]Time required for the plasma concentration of MTK to decrease to half of C_{max}. [b]Time required for half of the plasma MTK to be removed during the terminal elimination phase. The elimination phase ranged from 7 to 28 days. Data represent the mean ± SD (n = 5). Statistical analysis was conducted using one-way ANOVA variance. *$p < 0.05$, compared to 3MS.
Abbreviations: MTK, montelukast; SC, subcutaneous; NS, nanocrystalline suspension; MS, microcrystalline suspension; C_{max}, maximum plasma concentration; T_{max}, time to peak maximum plasma concentration; AUC, area under the plasma concentration versus time curve; $T_{1/2}$, half-life.

Currently, clinical trials of MTK oral therapy for the treatment of Alzheimer's disease have been conducted with oral dose of 10–40 mg once daily.[14] In pharmacokinetic study in human, C_{max} value was reached to 500 ng/mL with an oral dose of 10 mg/day, with the trough concentration over 18 ng/mL.[69,70] Therefore, the primary goal of the novel prolonged delivery system was to provide plasma concentration of MTK over 20 ng/mL following a single administration. As shown in Figure 4A, the drug concentration in the plasma was rapidly elevated within 1 day following the MTK suspension. After the 200 and 500NS injection, C_{max} was determined to be 298 and 370 ng/mL, respectively; and that of 3MS was 200 ng/mL, with no marked statistical difference. This result corresponds to the aforementioned in vitro dissolution profiles. MTK nanocrystals provided faster dissolution by an interstitial fluid at the injection site and were distributed into the bloodstream in tissues compared to microcrystals.[24] Considering the C_{max} value of the current oral therapy (10 mg/day) in humans is more than 500 ng/mL,[70] the C_{max} obtained with NSs (<400 ng/mL at a dose 30 mg/kg in rats) was considered to be tolerable. Concerning the 200NS and 500NS, the plasma drug concentration declined rapidly for 2 days after reaching the peak, with the elimination $T_{1/2(\alpha)}$ of 0.2 and 0.8 days in 200NS and 500NS, respectively. In contrast, the MTK plasma concentration decreased more slowly in the presence of 3MS, with a $T_{1/2(\alpha)}$ of 3.7 days. The drug concentrations from injectable MTK systems slowly declined but maintained plasma concentrations >50 ng/mL over 14 days in all formulations (200NS, 500NS, and 3MS). Afterward, the MTK concentration gradually decreased, and its plasma concentration was <10 ng/mL in all crystal formulations after 28 days. The elimination half-life from days 7 to 28 post-dosing ($T_{1/2(\beta)}$) was 4.0–7.8 days, with no significant difference. There was no marked difference between the crystal formulas in the AUC (0–28 days) value, a pharmacokinetic parameter representing drug absorption. The $AUC_{(0-28\ days)}$ following 200NS, 500NS, and 3MS SC injection was 1418.3, 1737.2, and 1533. ng·day/mL, respectively. This indicates that the administered drug crystals provided an equivalent extent of drug absorption despite the differences in absorption rates.

Histopathological Observation Following SC Injection of MTK Suspension in Rats

The H&E-stained subcutaneous tissues injected with normal saline, 200NS, 500 NS, and 3MS were observed histologically to compare the local inflammatory response and further understand the pharmacokinetic profile of MTK. Thomaidou et al 2019 reported that up to 40% of self-injectable SC injections registered by the Food and Drug Administration (FDA) cause adverse reactions at the injection site.[71] In particular, injection-site adverse effects such as pain, bruising, swelling, or granuloma have been reported as one of the most commonly reported adverse events in long-acting suspension clinical studies.[20,23] Moreover, local inflammatory responses at the injection sites have recently been recognized as important factors that affect drug absorption profiles and local tolerability. According to Darville et al,[72] IM-injected paliperidone palmitate crystals (~1000 nm) elicited an injection site reaction consisting of acute inflammation, followed by a chronic inflammatory response.[73,74] Drug dissolution proceeded rapidly and profoundly within 24 h, with acute edema and swelling at the injection site, resulting in a rapid increase in plasma paliperidone levels. A subsequent chronic granulomatous

inflammation characterized by infiltration of inflammatory cells derived from the blood, drug crystal phagocytosis by macrophages, granulation, and a dense inflammatory envelope places the drug crystals in macrophage-associated secondary depots, retarding drug dissolution and absorption rates.

In this study, the injection of equal volumes of vehicle solution did not cause histological changes or tissue responses in the surrounding tissues during the experimental period (Figure 7). In contrast, a granulomatous inflammation response associated with macrophage infiltration, granulocytes, fibroblasts, lymphocytes, and plasma cells was observed at the injection site in all MTK particle-administered groups (Figure 7). Four days after dosing, widespread necrotic areas surrounded by inflammatory bands, such as polymorphonuclear leukocytes (PMNs) and lymphocytes, were observed in all MTK particle-injection sites, regardless of particle size. On day 7 after dosing, the necrotic area was noticeably decreased, with distinct chronic inflammatory cell infiltration, including lymphocytes and macrophages. Moreover, granulation tissue formation around the injection site was observed with increased fibroblast proliferation and new blood vessel formation. This is consistent with a previous report that moderate to marked mononuclear cell infiltration (mainly activated macrophages) was the dominant feature in the inflammatory rim of an IM-injected paliperidone palmitate drug suspension, 1–14 days post-dosing.[72] This fibrous encapsulation process with interfacial foreign-body reactions isolated the drug crystal from the intestinal fluids or capillaries, impeding MTK particle dissolution and affording a protracted pharmacokinetic profile 4 days after SC injection (Figure 7). Fourteen days post-dosing, the depot and surrounding inflammatory lesions began to alleviate in all MTK crystal-treated groups gradually. Necrotic areas were mostly removed and replaced with macrophages and multifocally infiltrated lymphocytes. Fibroblast proliferation and angiogenesis were also observed. After 28 days of injection, most local inflammation responses and necrosis at the injection site were diminished in all MTK-treated groups, as most MTK crystals were dissolved and
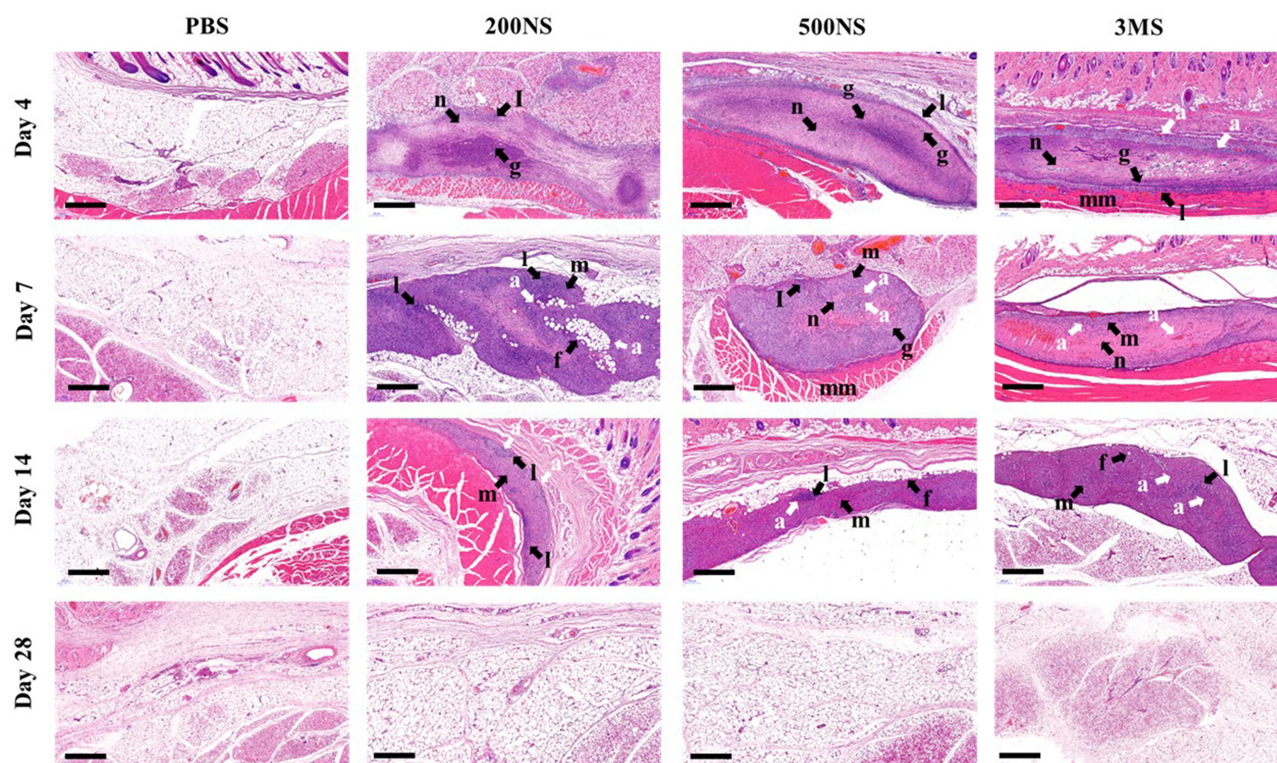
Figure 7 Histopathologic observation of the H&E-stained administration site following SC injection of PBS (negative control) and MTK crystalline suspensions (200NS, 500NS, and 3MS) in rats.
Notes: Scale bars indicate 600 μm. Photomicrographs of HE-stained cross-sections show progressive foreign body reactions, such as necrosis, macrophage infiltration, fibrosis, and angiogenesis, in the montelukast nanocrystal suspension-injected groups. Black arrows indicate the necrotic area (n), granulocyte infiltration (g), lymphocyte infiltration (l), macrophages (m), and infiltrated adipocytes (f). Additional noteworthy features such as active capillaries and angiogenesis (a) are marked with white arrows.
Abbreviations: H&E, hematoxylin, and eosin; SC, subcutaneous; PBS, phosphate-buffered saline; MTK, montelukast; 200NS, 200 nm-sized nanocrystalline suspensions; 500NS, 200 nm-sized nanocrystalline suspensions; 3MS, 3 μm-sized microcrystalline suspensions.
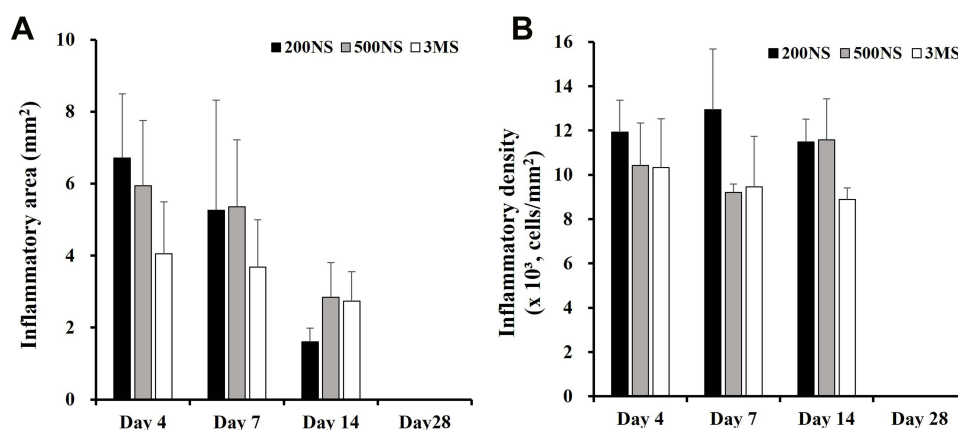
Figure 8 Temporal evolution of (**A**) inflammatory area (mm^2) and (**B**) inflammatory density (cells/mm^2) following SC injection of MTK crystalline suspensions in rats.
Notes: Each point in the graph represents mean ± SD (n = 4). Quantitative histopathological data were acquired using QuPath software by calibrating and analyzing microscopic images of H&E-stained sections.
Abbreviations: SC, subcutaneous; MTK, montelukast; 200NS, 200 nm-sized nanocrystalline suspensions; 500NS, 200 nm-sized nanocrystalline suspensions; 3MS, 3 μm-sized microcrystalline suspensions; H&E, hematoxylin, and eosin.

gradually absorbed into the bloodstream. This histological observation corresponds to the previous MTK pharmacokinetic profile, showing its disappearance in the bloodstream after weeks, regardless of particle size.

Quantification of Inflammatory Cells Infiltrated at the Injection Site

Depending on the particle size, the degree of inflammatory cell infiltration at the injection site was comparatively evaluated based on the inflammatory area (mm^2) and the number of total inflammatory cells at the injection site (Figure 8). When assessing the inflammatory area 4 days after SC injection of MTK particles using the Caseviewer program, 200NS (6.70 mm^2) and 500NS (5.90 mm^2) exhibited larger inflammatory areas than 3MS (4.04 mm^2). MTK nanocrystals were widespread over the subcutaneous tissue, with lower viscosity and higher diffusion rate, due to their smaller particle size. Subsequently, the inflammatory area gradually decreased over 7, 14, and 28 days in all groups. Most inflammatory lesions resolved after 4 weeks, as confirmed by previous histopathological observations.

Next, the inflammatory cell infiltration density per lesion (cell/cm^2) was evaluated by determining the total number of inflammatory cells in the H&E-stained images using the QuPath program. The total number of inflammatory cells included macrophages, neutrophils, and monocytes. Darville et al revealed that the infiltrated mononuclear cells were mainly CD68$^+$ macrophages from vascular origins following IM injection of paliperidone palmitate nanocrystals.[72] In this study, the infiltration density of inflammatory cells was comparable between the groups, with no marked differences depending on the particle size. Four days post-dosing, macrophages were infiltrated at a density of $10–12 \times 10^3$ cells/mm^2 and upheld for 14 days, with a density of about $8–12 \times 10^3$ cells/mm^2. At 28 days post-dosing, the inflammatory cell density rapidly decreased, and the inflammatory lesion almost resolved, with the removal of MTK crystalline at injection site. We concluded that the characteristic chronic granulomatous inflammation response against MTK particles was deeply associated with extended pharmacokinetic profile following SC injection, and the transient local inflammatory response was recoverable as the loss of drug particles at the injection site.

Conclusion

The novel MTK parenteral delivery system was designed to provide an extended pharmacokinetic profile and better compliance in patients with Alzheimer's disease. Amorphous MTK powder was effectively converted into a crystalline form through solvent-mediated transformation, drastically decreasing the dissolution rate in physiological media. Subsequently, 200, 500, and 3000 nm-sized MTK crystalline suspensions with distinctive crystalline forms were prepared using the lab-scale bead milling method. The prepared nanoformulations provided a lengthened drug concentration–time profile in plasma for up to 4 weeks following a single SC injection in rats. Moreover, histopathological observations

showed that granulomatous inflammation caused by the MTK nanocrystal injection was transient and recoverable after 4 weeks, regardless of particle size. Therefore, the novel MTK NS system is expected to be a potent tool for improving adherence in patients with Alzheimer's disease.

Acknowledgments

Disclosure

The authors report no conflicts of interest.

References

1. Alzheimer's Disease Facts and Figures. 2020 Alzheimer's disease facts and figures. *Alzheimers Dement*. 2020;16(3):391–460. doi:10.1002/alz.12068
2. Giovannini J, Smeralda W, Jouanne M, Sopkova-de Oliveira Santos J, Catto M, Voisin-Chiret AS. Tau protein aggregation: key features to improve drug discovery screening. *Drug Discov Today*. 2022;27(5):1284–1297. doi:10.1016/j.drudis.2022.01.009
3. DeTure MA, Dickson DW. The neuropathological diagnosis of Alzheimer's disease. *Mol Neurodegeneration*. 2019;14:32. doi:10.1186/s13024-019-0333-5
4. Rahdaman MM, Lendel C. Extracellular protein components of amyloid plaques and their roles in Alzheimer's disease pathology. *Mol Neurodegener*. 2021;16(1):59. doi:10.1186/s13024-021-00465-0
5. Mukhin VN, Pavlov KI, Klimenko VM. Mechanisms of neuron loss in Alzheimer's disease. *Neurosci Behav Physi*. 2017;47:508–516. doi:10.1007/s11055-017-0427-x
6. Leng F, Edison P. Neuroinflammation and microglial activation in Alzheimer disease: where do we go from here? *Nat Rev Neurol*. 2020;17(3):157–172. doi:10.1038/s41582-020-00435-y
7. Heppner FL, Ransohoff RM, Becher B. Immune attack: the role of inflammation in Alzheimer disease. *Nat Rev Neurosci*. 2015;16(6):358–372. doi:10.1038/nrn3880
8. Zhao R, Ying M, Gu S, et al. Cysteinyl leukotriene receptor 2 is involved in inflammation and neuronal damage by mediating microglia M1/M2 polarization through NF-κB pathway. *Neuroscience*. 2019;422:99–118. doi:10.1016/j.neuroscience.2019.10.048
9. Wang Y, Yang Y, Zhang S, Li C, Zhang L. Modulation of neuroinflammation by cysteinyl leukotriene 1 and 2 receptors: implications for cerebral ischemia and neurodegenerative diseases. *Neurobiol Aging*. 2020;87:1–10. doi:10.1016/j.neurobiolaging.2019.12.013
10. Lai J, Mei ZL, Wang H, et al. Montelukast rescues primary neurons against Aβ1-42-induced toxicity through inhibiting CysLT1R-mediated NF-κB signaling. *Neurochem Int*. 2014;75:26–31. doi:10.1016/j.neuint.2014.05.006
11. Datusalia AK, Singh G, Yadav N, Gaun S, Manik M, Singh RK. Targeted delivery of montelukast for treatment of Alzheimer's disease. *CNS Neurol Disord Drug Targets*. 2021. doi:10.2174/1871527320666210902163756
12. Xiong LY, Ouk M, Wu CY, et al. Leukotriene receptor antagonist use and cognitive decline in normal cognition, mild cognitive impairment, and Alzheimer's dementia. *Alzheimers Res Ther*. 2021;13(1):147. doi:10.1186/s13195-021-00892-7
13. IntelGenx Corp. Safety, and efficacy of a new buccal film of montelukast in patients with mild to moderate Alzheimer's disease (BUENA). Available from: https://clinicaltrials.gov/ct2/show/study/NCT03402503?term=montelukast&cond=Alzheimer+DiseaDi&draw=2&rank=2.identifier: NCT03402503. Accessed May 10, 2022.
14. Ihab Hajjar, Emory University. Montelukast therapy on Alzheimer's disease. Available from: https://clinicaltrials.gov/ct2/show/NCT03991988?term=montelukast&cond=Alzheimer+Disease&draw=2&rank=1.identifier:NCT03991988. Accessed May 10, 2022.
15. Cummings J, Lee G, Ritter A, Sabbagh M, Zhong K. Alzheimer's disease drug development pipeline: 2019. *Alzheimers Dement*. 2019;5:272–293. doi:10.1016/j.trci.2019.05.008
16. DrugBank. Montelukast sodium. Available from: https://go.drugbank.com/salts/DBSALT001043. Accessed August 23, 2022.
17. RXList. Singulair. Available from: https://www.rxlist.com/singulair-drug.htm#description. Accessed August 23, 2022.
18. Small G, Dubois B. A review of compliance to treatment in Alzheimer's disease: potential benefits of a transdermal patch. *Curr Med Res Opin*. 2007;23(11):2705–2713. doi:10.1185/030079907x233403
19. Ahmed TA, Ibrahim HM, Samy AM, et al. Biodegradable injectable in situ implants and microparticles for sustained release of montelukast: in vitro release, pharmacokinetics, and stability. *AAPS PharmSciTech*. 2014;15(3):772–780. doi:10.1208/s12249-014-0101-3
20. Shi Y, Lu A, Wang X, Belhadj Z, Wang J, Zhang Q. A review of existing strategies for designing long-acting parenteral formulations: focus on underlying mechanisms, and future perspectives. *Acta Pharm Sin B*. 2021;11(8):2396–2415. doi:10.1016/j.apsb.2021.05.002
21. Ho MJ, Jeong MY, Jeong HT, et al. Effect of particle size on in vivo performances of long-acting injectable drug suspension. *J Control Release*. 2022;341:533–547. doi:10.1016/j.jconrel.2021.12.011
22. Li W, Tang J, Lee D, et al. Clinical translation of long-acting drug delivery formulations. *Nat Rev Mater*. 2022;7:406–420.
23. Prabhakar C, Krishna K. A review on nanosuspensions in drug delivery. *Int J Pharma Bio Sci*. 2011;2(1):549–558.
24. Zuidema J, Kadir F, Titulaer HAC, Oussoren C. Release and absorption rates of intramuscularly and subcutaneously injected pharmaceuticals (II). *Int J Pharm*. 1994;105(3):189–207. doi:10.1016/0378-5173(94)90103-1
25. Darville N, van Heerden M, Mariën D, et al. The effect of macrophage and angiogenesis inhibition on the drug release and absorption from an intramuscular sustained-release paliperidone palmitate suspension. *J Control Release*. 2016;230:95–108. doi:10.1016/j.jconrel.2016.03.041
26. Chamanza R, Darville N, van Heerden M, De Jonghe S. Comparison of the local tolerability to 5 long-acting drug nanosuspensions with different stabilizing excipients, following a single intramuscular administration in the rat. *Toxicol Pathol*. 2018;46(1):85–100. doi:10.1177/0192623317737295

27. Nicoud L, Licordari F, Myerson AS. Estimation of the solubility of metastable polymorphs: a Critical Review. *Cryst Growth Des*. 2018;18 (11):7228–7237. doi:10.1021/acs.cgd.8b01200

28. Sadar MJ, Cox SK, Duvall A, Jones MP. Pharmacokinetics of a single intramuscular injection of ceftiofur crystalline free acid in bald eagles (Haliaeetus leucocephalus). *J Avian Med Surg*. 2021;35(3):290–294.

29. Chmiel K, Knapik-Kowalczuk J, Jurkiewicz K, Sawicki W, Jachowicz R, Paluch M. A new method To identify physically stable concentration of amorphous solid dispersions (I): case of flutamide + Kollidon VA64. *Mol Pharm*. 2017;14(10):3370–3380. doi:10.1021/acs.molpharmaceut.7b00382

30. Grzybowska K, Chmiel K, Knapik-Kowalczuk J, Grzybowski A, Jurkiewicz K, Paluch M. Molecular factors governing the liquid and glassy states recrystallization of celecoxib in binary mixtures with excipients of different molecular weights. *Mol Pharm*. 2010;14(4):1154–1168. doi:10.1021/acs.molpharmaceut.6b01056

31. Murdande SB, Pikal MJ, Shanker RM, Bogner RH. Aqueous solubility of crystalline and amorphous drugs: challenges in measurement. *Pharm Dev Technol*. 2011;16(3):187–200. doi:10.3109/10837451003774377

32. Newman A, Knipp G, Zografi G. Assessing the performance of amorphous solid dispersions. *J Pharm Sci*. 2012;101(4):1355–1377. doi:10.1002/jps.23031

33. Guo M, Sun X, Chen J, Cai T. Pharmaceutical cocrystals: a review of preparations, physicochemical properties and applications. *Acta Pharm Sin B*. 2021;11(8):2537–2564. doi:10.1016/j.apsb.2021.03.030

34. Zhang GG, Law D, Schmitt EA, Qiu Y. Phase transformation considerations during process development and manufacture of solid oral dosage forms. *Adv Drug Deliv Rev*. 2004;56(3):371–390. doi:10.1016/j.addr.2003.10.009

35. Zhu M, Wang Y, Li F, et al. Theoretical model and experimental investigations on solution-mediated polymorphic transformation of theophylline: from polymorph I to polymorph II. *Crystals*. 2019;9(5):260. doi:10.3390/cryst9050260

36. Steiner D, Bunjes H. Influence of process and formulation parameters on the preparation of solid lipid nanoparticles by dual centrifugation. *Int J Pharm*. 2021;3:100085. doi:10.1016/j.ijpx.2021.100085

37. Hagedorn M, Liebich L, Bögershausen A, et al. Rapid development of API nano-formulations from screening to production combining dual centrifugation and wet agitator bead milling. *Int J Pharm*. 2019;565:187–198. doi:10.1016/j.ijpharm.2019.04.082

38. Okafor NI, Nkanga CI, Walker RB, et al. Encapsulation and physicochemical evaluation of efavirenz in liposomes. *J Pharm Investig*. 2020;50:201–208. doi:10.1007/s40005-019-00458-8

39. Im SH, Jung HT, Ho MJ, et al. Montelukast nanocrystals for transdermal delivery with improved chemical stability. *Pharmaceutics*. 2019;12(1):18. doi:10.3390/pharmaceutics12010018

40. Erdoğar N, Akkın S, Nielsen TT, et al. Development of oral aprepitant-loaded chitosan–polyethylene glycol-coated cyclodextrin nanocapsules: formulation, characterization, and pharmacokinetic evaluation. *J Pharm Investig*. 2021;51:297–310. doi:10.1007/s40005-020-00511-x

41. Shamarekh KS, Gad HA, Soliman ME, et al. Towards the production of monodisperse gelatin nanoparticles by modified one step desolvation technique. *J Pharm Investig*. 2020;50:189–200. doi:10.1007/s40005-019-00455-x

42. Lee Y, Gurnon AK, Bodner D, et al. Effect of particle spreading dynamics on powder bed quality in metal additive manufacturing. *Integr Mater Manuf Innov*. 2020;9:410–422. doi:10.1007/s40192-020-00193-1

43. Kim DY, Lee HC, Jang YJ, et al. A simple and efficient method to determine montelukast in rat plasma using liquid-liquid extraction and tandem mass spectrometry. *Mass Spectrom Lett*. 2020;11(4):71–76. doi:10.5478/MSL.2020.11.4.71

44. Bankhead P, Loughrey MB, Fernández JA, et al. QuPath: open source software for digital pathology image analysis. *Sci Rep*. 2017;7:16878. doi:10.1038/s41598-017-17204-5

45. Acs B, Ahmed FS, Gupta S, et al. An open source automated tumor infiltrating lymphocyte algorithm for prognosis in melanoma. *Nat Commun*. 2019;10:5440. doi:10.1038/s41467-019-13043-2

46. Stritt M, Stalder AK, Vezzali E. Orbit image analysis: an open-source whole slide image analysis tool. *PLoS Comput Biol*. 2020;16(2):e1007313. doi:10.1371/journal.pcbi.1007313

47. Morris KR, Griesser UJ, Eckhardt CJ, Stowell JG. Theoretical approaches to physical transformations of active pharmaceutical ingredients during manufacturing processes. *Adv Drug Deliv Rev*. 2001;48:91–111. doi:10.1016/S0169-409X(01)00100-4

48. Aucamp ME, Stieger N, Barnard N, Liebenberg W. Solution-mediated phase transformation of different roxithromycin solid-state forms: implication in dissolution and solubility. *Int J Pharm*. 2013;449:18–27. doi:10.1016/j.ijpharm.2013.03.048

49. Liedtke S, Wissing S, Müller RH, Mäder K. Influence of high pressure homogenisation equipment on nanodispersions characteristics. *Int J Pharm*. 2000;196(2):183–185. doi:10.1016/S0378-5173(99)00417-2

50. Jacob S, Nair AB, Shah J. Emerging role of nanosuspensions in drug delivery systems. *Biomater Res*. 2020;24:3. doi:10.1186/s40824-020-0184-8

51. Niwa T, Miura S, Danjo K. Universal wet-milling technique to prepare oral nanosuspension focused on discovery and preclinical animal studies - Development of particle design method. *Int J Pharm*. 2011;405(1–2):218–227. doi:10.1016/j.ijpharm.2010.12.013

52. Kim EA, Park JS, Kim MS, et al. High-payload nanosuspension of centella asiatica extract for improved skin delivery with no irritation. *Int J Nanomedicine*. 2021;16:7417–7432. doi:10.2147/IJN.S335039

53. Kim H, Park H, Lee SJ. Effective method for drug injection into subcutaneous tissue. *Sci Rep*. 2017;9613. doi:10.1038/s41598-017-10110-w

54. McGuckin MB, Wang J, Ghanma R, et al. Nanocrystals as a master key to deliver hydrophobic drugs via multiple administration routes. *J Control Release*. 2022;345:334–353. doi:10.1016/j.jconrel.2022.03.012

55. Kwade A. Wet comminution in stirred media mills–Research and its practical application. *Powder Technol*. 1999;105:14–20. doi:10.1016/S0032-5910(99)00113-8

56. Merisko-Liversidge E, Liversidge GG, Cooper ER. Nanosizing: a formulation approach for poorly-water-soluble compounds. *Eur J Pharm Sci*. 2003;18:113–120. doi:10.1016/S0928-0987(02)00251-8

57. Kostanski JW; inventor; Otsuka Pharmaceutical Co., Ltd., assignee. Controlled release sterile injectable aripiprazole formulation and method. United States patent US7807680B2. 2020 Oct 5.

58. Malhotra G, Singh S, Ansari KA. Paliperidone palmitate particles and compositions thereof. World intellectual property organization. WO2016199170; 2016.

59. Paquette SM, Dawit H, Hickey MB, Merisko-Liversidge E, Almarsson O, Deaver DR. Long-acting atypical antipsychotics: characterization of the local tissue response. *Pharm Res*. 2014;31(8):2065–2077. doi:10.1007/s11095-014-1308-4

60. Mundhra DB; inventor; VIIV Healthcare Company, assignee. Pharmaceutical compositions. United States patent US20130171214A1. 2013 Jul 4.

61. Paredes AJ, Camacho NM, Schofs L, et al. Ricobendazole nanocrystals obtained by media milling and spray drying: pharmacokinetic comparison with the micronized form of the drug. *Int J Pharm*. 2020;585:119501. doi:10.1016/j.ijpharm.2020.119501

62. Bide Y, Fashapoyeh MA, Shokrollahzadeh S. Structural investigation and application of Tween 80-choline chloride self-assemblies as osmotic agent for water desalination. *Sci Rep*. 2021;11:17068. doi:10.1038/s41598-021-96199-6

63. Noyes AA, Whitney WR. The rate of solution of solid substances in their own solutions. *J Am Chem Soc*. 1897;19(12):930–934. doi:10.1021/ja02086a003

64. Abdelghany S, Tekko IA, Vora L, Larrañeta E, Permana AD, Donnelly RF. Nanosuspension-based dissolving microneedle arrays for intradermal delivery of curcumin. *Pharmaceutics*. 2019;11(7):308. doi:10.3390/pharmaceutics11070308

65. Junghanns JU, Müller RH. Nanocrystal technology, drug delivery and clinical applications. *Int J Nanomedicine*. 2008;3(3):295–309. doi:10.2147/ijn.s595

66. Shariare MH, Altamimi MA, Marzan AL, et al. In vitro dissolution and bioavailability study of furosemide nanosuspension prepared using design of experiment (DoE). *Saudi Pharm J*. 2019;27(1):96–105. doi:10.1016/j.jsps.2018.09.002

67. Thakkar HP, Patel BV, Thakkar SP. Development and characterization of nanosuspensions of olmesartan medoxomil for bioavailability enhancement. *J Pharm Bioallied Sci*. 2011;3(3):426–434. doi:10.4103/0975-7406.84459

68. He J, Han Y, Xu G, et al. Preparation and evaluation of celecoxib nanosuspensions for bioavailability enhancement. *RSC Adv*. 2017;7 (22):13053–13064. doi:10.1039/C6RA28676C

69. Zhao JJ, Rogers JD, Holland SD, et al. Pharmacokinetics and bioavailability of montelukast sodium (MK-0476) in healthy young and elderly volunteers. *Biopharm Drug Dispos*. 1997;18(9):769–777. doi:10.1002/(sici)1099-081x(199712)18:9<769::aid-bdd60>3.0.co;2-k

70. Graff GR, Weber A, Wessler-Starman D, Smith AL. Montelukast pharmacokinetics in cystic fibrosis. *J Pediatr*. 2003;142(1):53–56. PMID: 12520255. doi:10.1067/mpd.2003.mpd0332

71. Thomaidou E, Ramot Y. Injection site reactions with the use of biological agents. *Dermatol Ther*. 2019;32(2):e12817. doi:10.1111/dth.12817

72. Darville N, van Heerden M, Vynckier A, et al. Intramuscular administration of paliperidone palmitate extended-release injectable microsuspension induces a subclinical inflammatory reaction modulating the pharmacokinetics in rats. *J Pharm Sci*. 2014;103(7):2072–2087. doi:10.1002/jps.24014

73. Surve DH, Jindal AB. Recent advances in long-acting nanoformulations for delivery of antiretroviral drugs. *J Control Release*. 2020;324:379–404. doi:10.1016/j.jconrel.2020.05.022

74. Leng D, Chen H, Li G, et al. Development and comparison of intramuscularly long-acting paliperidone palmitate nanosuspensions with different particle size. *Int J Pharm*. 2014;472(1–2):380–385. doi:10.1016/j.ijpharm.2014.05.052